

Contents lists available at ScienceDirect

Acta Materialia

journal homepage: www.elsevier.com/locate/actamat



Full length article

Electron and phonon thermal conductivity in high entropy carbides with variable carbon content



Christina M. Rost^{a,b}, Trent Borman^c, Mohammad Delower Hossain^c, Mina Lim^d, Kathleen F. Quiambao-Tomko^e, John A. Tomko^e, Donald W. Brenner^d, Jon-Paul Maria^c, Patrick E. Hopkins ^{a,e,f,*}

- ^a Department of Mechanical and Aerospace Engineering, University of Virginia, Charlottesville, VA 22904, USA
- b Department of Physics and Astronomy, James Madison University, Harrisonburg, VA 22807, USA
- ^c Department of Materials Science and Engineering, The Pennsylvania State University, University Park, PA 16802, USA
- ^d Department of Materials Science and Engineering, North Carolina State University, Raleigh, NC 27695, USA
- e Department of Materials Science and Engineering, University of Virginia, Charlottesville, VA 22904, USA
- ^f Department of Physics, University of Virginia, Charlottesville, VA 22904, USA

ARTICLE INFO

Article history: Received 29 January 2020 Revised 10 May 2020 Accepted 2 June 2020 Available online 21 June 2020

ABSTRACT

Due to their diverse bonding character and corresponding property repertoire, carbides are an important class of materials regularly used in modern technologies, including aerospace applications and extreme environments, catalysis, fuel cells, power electronics, and solar cells. The recent push for novel materials has increased interest in high entropy carbides (HECs) for such applications. The extreme level of tunability alone makes HECs a significant materials platform for a variety of fundamental studies and functional applications. We investigate the thermal conductivity of high entropy carbide thin films as carbon stoichiometry is varied. The thermal conductivity of the HEC decreases with an increase in carbon stoichiometry, while the respective phonon contribution scales with elastic modulus as the excess carbon content increases. Based on the carbon content, the HECs transition from an electrically conducting metal-like material with primarily metallic bonding to a primarily covalently-bonded crystal with thermal conductivities largely dominated by the phononic sub-system. When the carbon stoichiometry is increased above this critical transition threshold dictating bonding character, the electronic contribution to thermal conductivity is minimized, and a combination of changes in microstructure, defect concentration and secondary phase formation, and stiffness influence the phononic contribution to thermal conductivity. Our results demonstrate the ability to tune the thermal functionality of high entropy materials through stoichiometries that dictate the type of bonding environment.

© 2020 Acta Materialia Inc. Published by Elsevier Ltd. All rights reserved.

1. Introduction

Somewhat analogous to medium and high entropy metallic alloys (HEAs) [1,2], the high entropy [3–6] and entropy-stabilized [7–9] family of ceramics contain four or more binary metal oxides (HEOs and ESOs), carbides (HECs), nitrides (HENs), or diborides (HEBs) in equimolar or near-equimolar concentrations, such that no particular element can be considered the principle component or host. Metal sublattice(s) can be randomly or preferentially occupied where configurational disorder is tailored on specific sites, while the non-metal sublattice remains site/element pure. To date,

E-mail addresses: phopkins@virginia.edu, phopkins@virginia.com (P.E. Hopkins).

several multicomponent and high entropy carbide systems have been successfully synthesized using spark plasma sintering (SPS) of component carbide powders [4,10–12]. Feng et al. [13] demonstrated the ability to synthesize HECs though carbothermal reduction of binary oxide precursors. Subsequent property studies have found increased oxidation resistance [14] and mechanical hardness values ranging from $\approx 10\%$ to $\approx 50\%$ [4,15,16] higher than that of their binary constituents. However, thermal conductivities of materials generally decrease with increasing number of elemental components, which is attributed to a combination of electron and phonon scattering from mass and interatomic force potential changes [7,17–21], and holds true for metal carbides [22–24]. As expected, higher order solid solutions result in lower thermal conductivities as mass and local structural disorder are introduced into the lattice.

^{*} Corresponding author at: Department of Mechanical and Aerospace Engineering, University of Virginia, Charlottesville, VA 22904, USA.

Typical carbide structures can be viewed as an arrangement of interstitial carbon in a simple metallic lattice. In many cases, carbides take on the cubic rocksalt or hexagonal structures. Deviations from ideal stoichiometry are quite common, and specific structural phases exist within a broad range of carbon content [22–24]. As such, point defects, particularly carbon vacancies and interstitials can have a dramatic effect on material properties. An important question to consider is how properties of high entropy carbide systems respond to deviations in carbon content. While the thermal properties of refractory ceramics are generally well-studied, explorations of high entropy carbide systems remain few and far between, especially with regard to carbon stoichiometry and defects.

Here, we characterize the thermal conductivity of novel high entropy carbide (HEC) thin films with nominal compositions $Hf_{0.2}Zr_{0.2}Ta_{0.2}Mo_{0.2}W_{0.2}C_{1-x} \ \ and \ \ Hf_{0.2}Zr_{0.2}Ta_{0.2}Ti_{0.2}Nb_{0.2}C_{1-x}, \ \ and$ their dependence on carbon stoichiometry, x. Our HECs can transition from electrically-conducting, with electrons dominating the thermal transport in a material with primarily metallic bonding, to ceramic-like systems with primarily covalent bonding, where thermal conductivities are largely dominated by the phononic subsystem and an increase in elastic modulus that depends on the amount of excess carbon in the HEC is observed. While the electronic contribution to thermal conductivity remains at a constant when the crystal is primarily covalently bonded, a combination of changes in film morphology, point defect scattering, and phase precipitation systematically lower the phononic contribution to thermal conductivity with further increased carbon content in the films.

2. Experimental methods and results

To facilitate the carbon content study with smoothly changing stoichiometry, we use sputter deposition as it affords this ability more easily than by powder processing routes. The carbon content in the HEC films is varied by controlling the methane flow rate and concomitant percent methane (% CH₄) in the deposition plasma; further details of film growth and characterization are discussed in the Supplemental Materials [25], with pertinent properties of the HEC films tabulated in Supplemental Tables S1 and S2. The results on composition $HfZrTaMoWC_{1-x}$ are presented here, with results on the HfZrTaTiNbC_{1-x} composition in the Supplemental Materials [25]. Structural and compositional characterization, using x-ray diffraction (XRD), scanning electron microscopy (SEM) and X-ray photoelectron spectroscopy (XPS), are shown in Fig. 1. XRD and SEM results, in Fig. 1a and c, respectively, were used to determine the phase and microstructure evolution of the thin films as methane flow was increased during deposition. At 2 sccm methane, the films exhibit a primary BCC metal phase with a possible secondary carbide, or carbon-rich metal phase. As flow is increased, these metallic phases evolve into a single-phase rocksalt shown in Fig. 1a, space group 225 (Fm3m), with lattice parameter a = 4.47 Å. Below 6 sccm methane, the SEM images show an equiaxed metallic microstructure. At 6 sccm, films form (111) textured carbide grains with no evidence of a remaining metallic phase in the XRD. As methane flow rate is increased past this point, the textured carbide grains begin to shrink and a nanocrystalline precipitate forms. There is no evidence of the nanocrystalline phase in the XRD at higher flow rates, possibly due to a small volume ratio compared to the primary carbide phase. We estimate the grain sizes in the primarily metallically-bonded HEC films as $\sim 100 \pm 20$ nm. As the flow rate is increased above 8 sccm, promoting a more covalently-bonded polycrystal, the average grain sizes decrease to $\sim\!20\pm10\,\text{nm}.$ These grain sizes were estimated from image analyses on the SEM micrographs and analyzing over 30 grains for each sample. In all cases, the films are free from visible pores.

XPS measurements provide insight regarding the carbon stoichiometry changes as a function of the methane present during film growth, shown in Fig. 1b. As expected, the total carbon content of the films increase as methane increases. The amount of carbon bonded to metals increases dramatically at first, leading to the transition from a primarily metallically-bonded system to a primarily covalently-bonded system, shown in XPS under 13% methane content. After reaching 80% stoichiometric carbide, the rate of bonded carbon within the films begins to lessen while excess carbon increases rapidly to a maximum of approximately 70%. Note, XPS depth profiling on various control samples ranging from hundreds of nanometers to micrometers confirm that our deposition process results no gradation in elemental composition through the thickness of the film. Thus, our XPS data, which measure the chemical composition on the surface of the sample, are indicative of the composition through the entire thickness of the film.

This transition in bonding character with increasing carbon content shown in our HECs in Fig. 1 also implies a change in the relative contribution of the primary energy carriers (i.e., electrons and phonons); in other words, the relative contribution of electrons and phonons to the thermal conductivity would change during the carbon stoichiometry-induced transition from primarily metallic bonding to primarily covalent bonding. The thermal conductivities of the thick HEC films (thicknesses $\sim 1-2 \mu m$), measured via time domain thermoreflectance (TDTR) [26,27], are shown in Fig. 2a as a function of methane content present during film deposition. A secondary thin film ($\approx 100 \, \text{nm}$ thick) series was grown and characterized in order to observe any size effects related to film thickness, shown in Fig. 2b. Details of this $HfZrTaMoWC_{1-x}$ film set are included in the Supplemental Material, along with thermal conductivity measurements on a different HEC composition thin film series (HfZrTaTiNbC_{1-x}) [25].

We approximate the electron contribution of the thermal conductivity, κ_e , to this measured thermal conductivity, $\kappa_{\rm total}$ (= κ_e + κ_p), by applying the Wiedemann-Franz Law [28] to electrical resistivity measurements of the thin films. We calculate κ_e using two different assumptions for the room temperature Lorentz number of our HEC films: the low-temperature Lorentz number ($L=L_0=2.44\times 10^{-8}~{\rm W}~{\rm X}~{\rm K}^{-2}$) and a temperature-dependent Lorentz number originally derived by Makinson [29] that accounts for electron-phonon and electron-impurity scattering, the results of which are shown in Fig. 2 and Fig. 3, respectively. We assume that these two approaches for calculated κ_e set the uncertainty in both κ_e and κ_p , described below.

The uncertainty in our calculation of the electrical contribution to the thermal conductivity, κ_e , of the HEC films calculated via the Wiedemann-Franz Law [28] is directly related to our assumption of the Lorentz number, L. The Wiedemann-Franz Law is given by $\kappa_e = \sigma LT$, where $\sigma = 1/\rho$ is the electrical conductivity (ρ is the electrical resistivity) and T is the absolute temperature. Thus the choice of L can strongly impact the derived κ_e . It is well established that the low temperature-derived value of $L = L_0$ can overpredict L at elevated temperatures below the Debye temperature (such as room temperature in metal carbides) [30,31]. At these elevated temperatures, inelastic electron-phonon scattering events (so called "vertical processes") can lead to values of L that are less than L_0 [29,32]. Previous works have shown that the compositional disorder in metallic alloys leads to increased elastic electron scattering events that can dominate over inelastic processes, thus rendering the use of $L = L_0$ at room temperature acceptable [33,34]. The HECs studied in this work are in fact random solid solutions, and thus we would expect similar elastic disorder scattering in the electronic system. Thus, we assume $L=L_0$ as our upper bound for electron thermal conductivities, and these data are plotted in Fig. 2 for the thick and thin HEC films, along with the corresponding values calculated for the phonon thermal conductivity, κ_p .

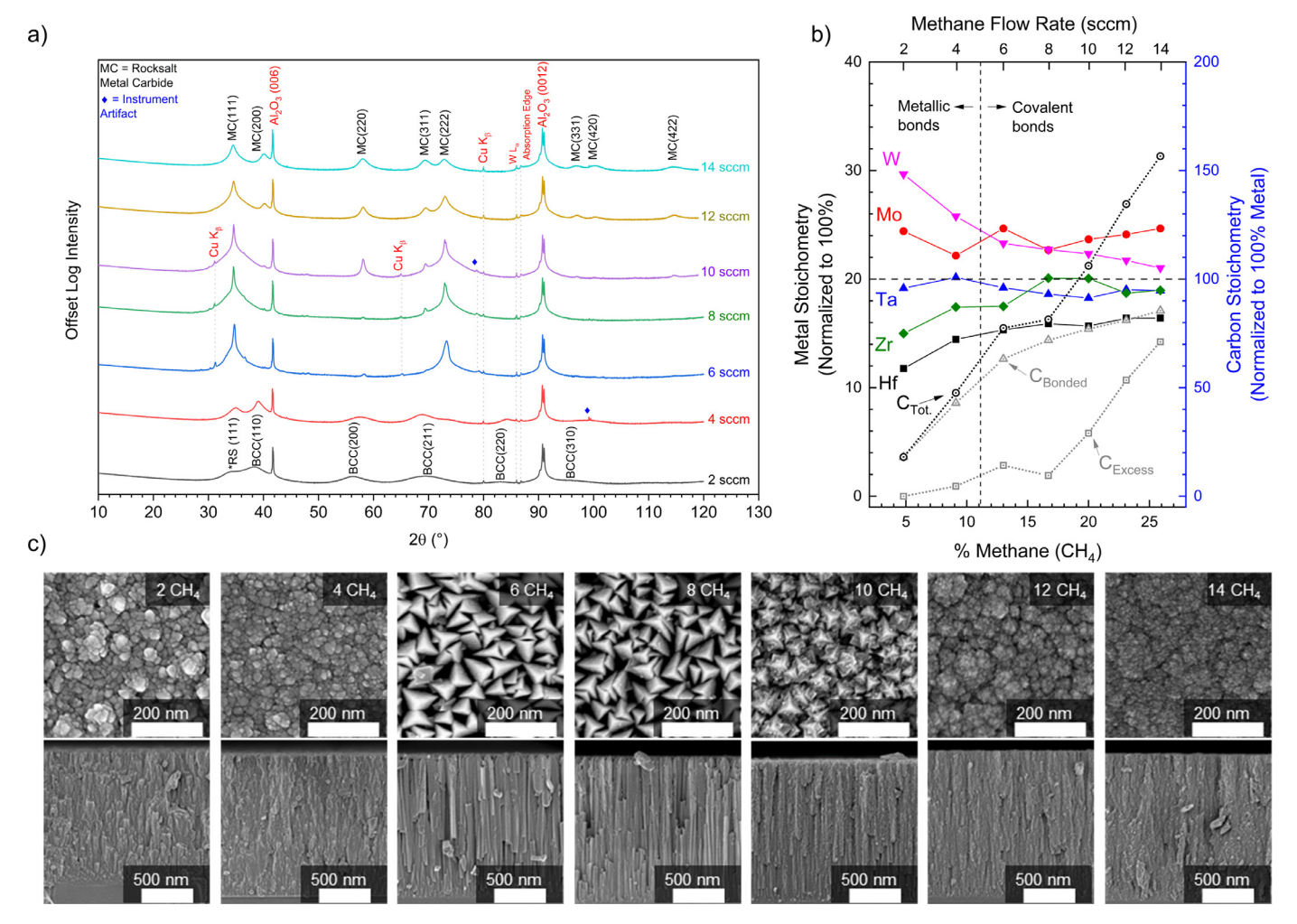


Fig. 1. Structural and chemical properties of the $Hf_{0.2}Zr_{0.2}Ta_{0.2}Mo_{0.2}W_{0.2}C_{1-x}$ thin films. (a) Offset XRD plot depicting carbide phase evolution as a function of methane flow rate during thin film deposition. (b) XPS data showing normalized metal and carbon stoichiometry plotted as a function of the methane flow rate. Total carbon is the sum of metal-bonded carbon and excess carbon. (c) SEM micrographs of HEC film microstructure evolution with increasing methane flow rate, shown for the thick HEC film series. Top row shows the plan view of microstructures while the bottom row corresponds to film cross-sections.

Conversely, however, single element metal carbides have been shown historically to have a lower Lorentz number than L_0 at room temperature due to a large residual resistivity from carbon vacancies [30]. In this case, the more rigorous form of the Lorentz number derived by Makinson [29] should be applied to the HECs to calculate L, given by

$$L_{\text{th}} = \frac{\rho_{\text{imp}} + \left(\frac{\Theta_D}{T}\right)^5 J_5 \left[\frac{\Theta_D}{T}\right]}{\rho_{\text{imp}} + \left(\frac{\Theta_D}{T}\right)^5 J_5 \left[\frac{\Theta_D}{T}\right] \left(1 + \frac{3}{\pi^2} \left(\frac{k_F}{q_D}\right)^2 \left(\frac{\Theta_D}{T}\right)^2 - \frac{1}{2\pi^2} \frac{J_7 \left[\frac{\Theta_D}{T}\right]}{J_5 \left[\frac{\Theta_D}{T}\right]}\right)}$$

$$(1)$$

where k_F is the Fermi wave vector, Θ_D is the Debye temperature, q_D is the Debye wave vector, $\rho_{\rm imp}$ is a term that accounts for electron-impurity scattering, and the Debye integrals, J_n are defined as

$$J_n \left[\frac{\Theta_D}{T} \right] = \int_0^{\frac{\Theta_D}{T}} \frac{x^n \exp\left[x\right]}{\left(\exp\left[x\right] - 1\right)^2} \, \mathrm{d}x. \tag{2}$$

To approximate $L_{\rm th}$ at room temperature for our HECs, we assume the Debye temperature is an average of the constituent metal carbides' Debye temperatures [36,37] (an assumption supported by our finding that the heat capacities of these HECs following a rule of mixtures [25], similar to our previous work on entropystabilized oxides [7]), $k_F/q_D=2^{-1/3}$ from free electron theory [32], and $\rho_{\rm imp}$ is approximated by taking the ratio of electrical resistivity of our lowest electrical resistance HEC to that of TaC at room temperature [38]. From these assumptions, we calculate $L_{\rm th}=0.65L_0$, and use this for our calculations of κ_e in Fig. 3 for the thick and thin HEC films, along with the corresponding values calculated for the phonon thermal conductivity, κ_p .

Thus, in this approach to calculate κ_e (and corresponding κ_p) for these HECs in two different ways using two different Lorentz numbers (L_0 in Fig. 2 and $L_{\rm th}=0.65L_0$ in Fig. 3) asserts that there are two bounds for the Lorentz number for these HECs: the upper bound being L_0 , which implies that disorder scattering makes the electronic thermal response behave more like a disordered metal, and the lower bound being $L_{\rm th}=0.65L_0$, which implies that the electronic thermal response will behave more like a single metal carbide. We use these bounds to also calculate the range of potential κ_p , setting the upper and lower limits of the phonon thermal conductivity in these HECs. These calculated phonon thermal conductivities are plotted along with the elastic modulus, E, of these

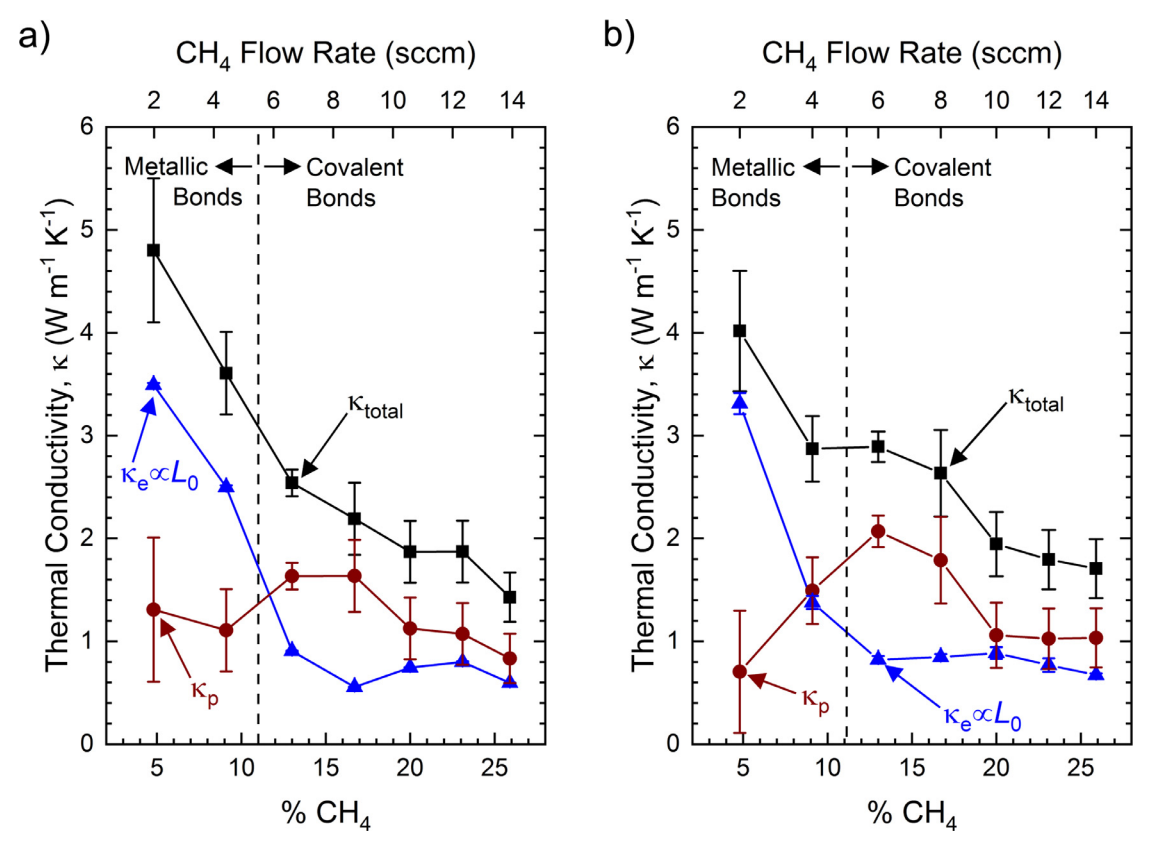


Fig. 2. Thermal conductivity of HfZrTaMoWC_{1-x} thin films measured with TDTR (κ_{total}) plotted as a function of methane flow rate in the deposition plasma (and corresponding % CH₄) during deposition for the a) thick ($\approx 1-2~\mu\text{m}$) film series and b) thin ($\approx 100~\text{nm}$) film series. Precise thicknesses for each film are tabulated in the Supplemental Materials [25]. The electrical contributions to the measured total thermal conductivity, κ_e , are calculated from the Wiedemann-Franz Law applied to electrical resistivity measurements on these films assuming the low temperature value for $L=L_0=2.44\times10^{-8}~\text{W}~\Omega~\text{K}^{-2}~[28,35]$, and thus in this figure, $\kappa_e \propto L_0$. The phonon contributions to the HEC thermal conductivities are then calculated as $\kappa_p = \kappa_{\text{total}} - \kappa_e$. These measurements of κ_{total} and resulting calculations of κ_e and κ_p show a cross-over from electron-dominated thermal conductivity to phonon-dominated thermal conductivity as the primary bonding character in the HEC films transition from metallic to covalent.

films as a function of ${\rm CH_4}$ flow rate in Fig. 4 and discussed in more detail in the next section.

We note that while these electrical resistivity measurements are taken in the in-plane direction, and the thermal conductivity measurements are dominated by cross-plane thermal transport, the cubic structure of these HECs and the ability for our thermal conductivity measurements to determine the intrinsic thermal conductivity without obfuscation from the thermal boundary conductance across the adjacent film interfaces warrant this comparison [39]. Even with the sample-varying grain size and microstructure, our assumption of isotropic electrical resistivity in these films, and thus in-plane and cross-plane electrical conduction being equal, is further supported based on the electronic mean free paths in these highly compositionally disordered metal carbides. Previous works have demonstrated that high entropy metallic alloys [40] and metal carbides [31] are known to have electron mean free paths on the order of nanometers or less at room temperature. Given that all of the HEC samples studied in this work have higher electrical resistivities than these previously reported high entropy metallic alloys [40] and typical metal carbides [30,41], we posit that the electron mean free paths in our HECs are on the order of 1 nm, which is at least an order of magnitude smaller than the smallest grain size that we measure in our HEC films. Thus, we do not expect the changing microstructure in these HEC films fabricated at different methane flow rates to obfuscate our assumption of isotropic electrical transport.

3. Discussion

The total and electronic thermal conductivities decrease as methane concentration increases. The phonon contribution to the thermal conductivity (derived from $\kappa_p = \kappa_{\rm total} - \kappa_e$) becomes the dominant thermal transport mechanism at 13% methane. At higher methane concentrations, the phonon contribution to thermal conductivity continuously decreases as the methane content in the deposition plasma is increased. These changes in κ_e and κ_p are related to the transition of the HEC from mostly metallic bonding to mostly covalent bonding, and dependent on not only electronic scattering with carbon defects, but could also be driven by lattice stiffening, density changes, and additional crystal quality considerations, as described below. It is noted that the trend remains consistent between the thick and the thin films series, suggesting the characteristics observed are intrinsic to the carbide system, and not dependent on film thickness.

In the primarily metallic films, κ_e plays a substantial, if not dominant role in the total thermal conductivity; regardless of our assumption of L when determining κ_e , our results show that the metallically-bonded films have a substantial electronic contribution to thermal conductivity, akin to that of a metal. When more carbon is introduced into the system, κ_e abruptly drops as carburization occurs and the films become primarily covalently-bonded. In this carbide phase, the cross over to a HEC system in which the thermal conductivity is phonon-dominated corresponds to where the ratio of metal-bonded carbon to excess carbon is maximized. Past this point, the accumulation of excess carbon degrades film quality in terms of primary carbide microstructure and secondary phase accumulation, as evidenced in SEM Fig. 1c, and ultimately reduces the thermal conductivity. The triangular-like grain growth observed in the HEC films deposited with 6 and 8 sccm methane shown in Fig. 1c are associated with epitaxial growth, thus implying the highest crystalline quality films are produced in this flow rate regime. This peak in crystal quality occurs in the

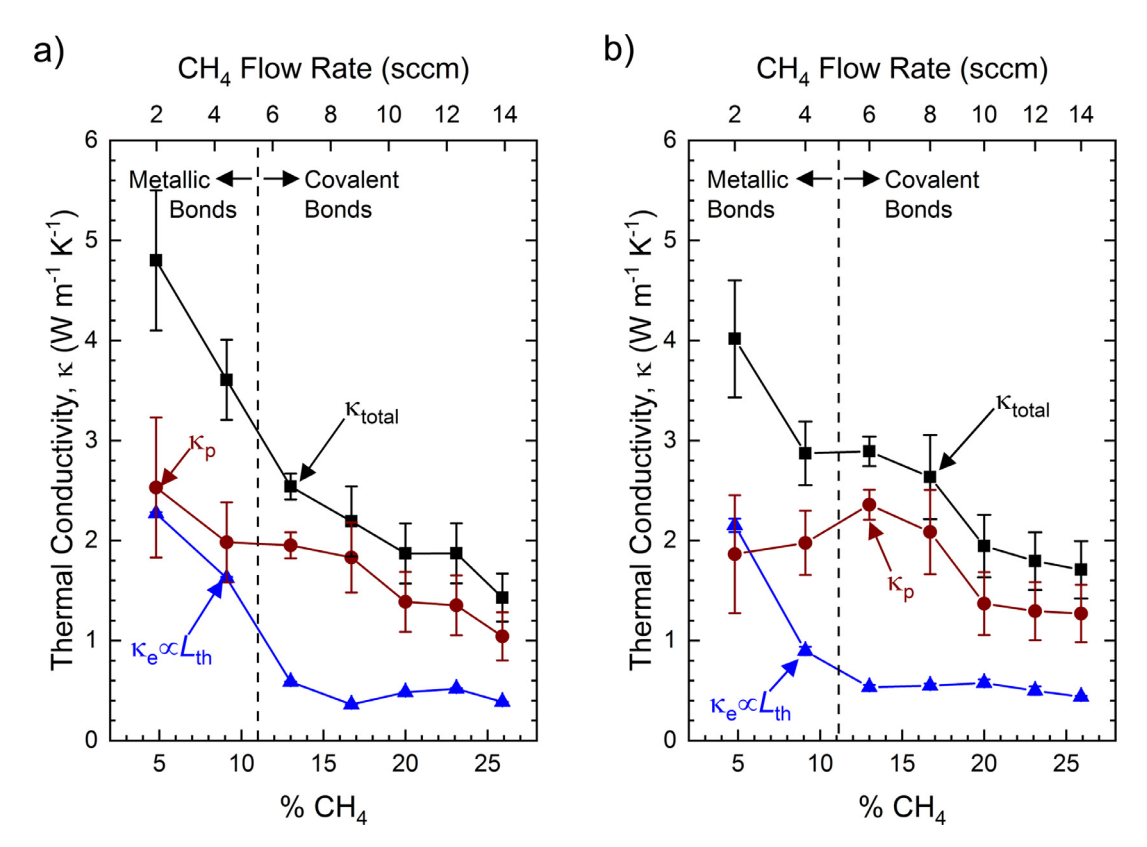


Fig. 3. Same as Fig. 2 only with κ_e calculated with the Lorentz number that accounts for inelastic electron-phonon scattering and electron-impurity scattering originally derived by Makinson [29] and given in Eq. (1), and thus $\kappa_e \propto L_{\rm th}$. Similar trends are observed here in κ_e and κ_p as in Fig. 2, in that we observe a cross-over from electron-dominated thermal conductivity to phonon-dominated thermal conductivity as the primary bonding character in the HEC films transition from metallic to covalent. The assumption of $L = L_0$ in the Wiedemann-Franz Law calculations of κ_e in Fig. 2 implies disorder scattering makes the electronic thermal response behave more like a pure disordered metal, while the use of $L = L_{\rm th}$ calculated via Eq. (1) implies that the electronic thermal response will behave more like a single metal carbide. The trends in thermal conductivity and this observed crossover from electron to phonon dominated thermal transport as the bonding character transitions from primarily metallic to covalent holds regardless of our assumption of L in the calculation of κ_e and subsequent κ_p .

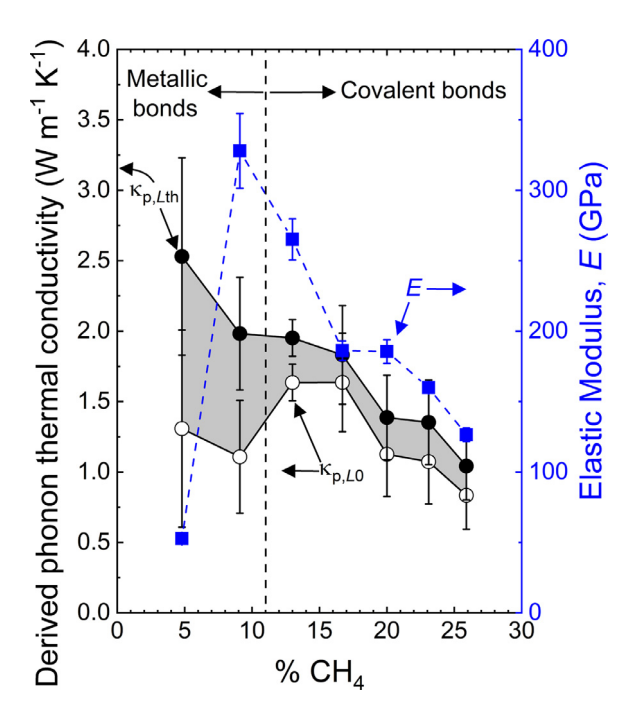


Fig. 4. Derived phonon thermal conductivity, κ_p , and elastic modulus, E, versus methane content for the thick HEC film series. We show κ_p calculated via either assuming $\kappa_e \propto L_0$ (c.f., Fig. 2) or $\kappa_e \propto L_{\rm th}$, where $L_{\rm th}$ is determined via Eq. (1) (c.f., Fig. 3). Regardless of Lorentz number assumption, we observe a reduction in κ_p with reduction in elastic modulus in the primarily covalently bonded regime in the thick HEC films.

films with the highest κ_p after the bonding becomes primarily covalent.

Crystal quality has been shown to directly impact thermal conductivity [42,43], and can be driven by several factors including point or line defects, and grain or phase boundaries. In the case of our HECs, an increase in flow rate beyond the 6-8 sccm regime leads to not only a decrease in grain size (spanning from $\sim 100 \pm 20$ nm for the 6 sccm films to $\sim 20 \pm 10$ nm for the highest sccm film), but also an increase in excess carbon content. Thus, one possible reason that κ_p decreases with increased flow rate once the bonding transitions to primarily covalent is that the mean free path of the phonons continues to decrease due to a higher rate of grain boundary and carbon point defect scattering.

We also note that the trend in derived phonon thermal conductivities with increased methane flow rate also correlates to the trends observed in the elastic modulus, measured though nanoindentation on the thick HEC films, shown in Fig. 4; note, this reduction in κ_p with reduction in elastic modulus in the primarily covalently bonded regime in the thick HEC films is observed regardless of our assumptions of L used when applying the Wiedemann-Franz Law. Thus, as the phonon thermal conductivity, κ_p is also related to the phonon energies and group velocities, i.e., the stiffness of the lattice, we also cannot rule out that changes in the modulus of the film are indicative of a changing atomic bonding environment that are thus impacting the thermal conductivity.

Additionally, the mass densities of the thin film HEC samples decrease as the methane content in the deposition plasma is increased. We measure the density of the $\sim\!100~\rm nm$ thin film HECs with X-ray reflectivity (XRR), and tabulate these values in Table S2

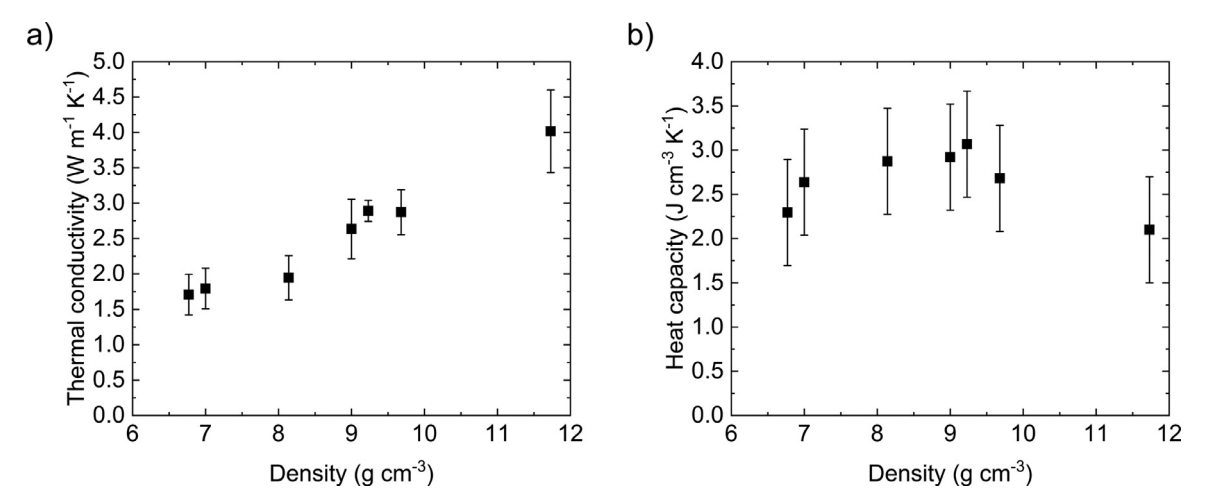


Fig. 5. (a) Thermal conductivity of the thin film HEC series as a function of mass density. (b) Volumetric heat capacity of the thin film HEC series as a function of mass density. These data are tabulated in Table S2.

in the Supplemental Material [25]. The thermal conductivities of these films increases monotonically with density, shown in Fig. 5a, which plots the TDTR-measured total thermal conductivities of the \sim 100 nm thin film HECs as a function of XRR-measured mass density. It is well established that the phonon thermal conductivity is proportional to the density [44] since the density is directly related to both heat capacity and the sound speed [35], which are directly related to the thermal conductivity (i.e., the Kinetic Theory approximation [45]).

This Kinetic Theory expression for thermal conductivity, given by $\kappa_p = C \nu \lambda / 3$, where *C* is the heat capacity, *v* is the velocity of the carriers, and λ is the mean free path, provides a platform to understand the mechanisms that are causing a reduction in the HEC phonon thermal conductivity with increased methane content in the deposition plasma in the primarily covalently-bonded regime. If the reduction of thermal conductivity were solely related to a change in the energies and velocities of the phonons, and not due to a changing mean free path, then κ_p would scale with changes in Cv (recall in the primarily covalently bonded regime, κ_p is the dominant mechanism of thermal transport in the HEC). The heat capacity is proportional to the mass density, ho, and inversely proportional to the atomic mass, M. Using TDTR, we also measure the heat capacities of these thin HEC films; we describe this process and TDTR sensitivities' to C in the Supplemental Material [25], but note that our measured heat capacities are dependent on our measured thermal conductivities, and thus have higher measurement uncertainties. Figure 5b plots the heat capacities of the thin film HECs as a function of mass density. Unlike the thermal conductivity, the heat capacities do not trend as strongly with density, however, we emphasize the larger uncertainties in these results. This is not necessarily surprising, since $C \propto \rho/M$, and while the mass density decreases in these HEC thin films, the carbon content is increased, so while ρ is decreasing, the average M of the HEC is also decreasing so the change in volumetric heat capacity is not expected to trend linearly with ρ . This also implies that the thermal conductivity changes of the HECs with changes in density are not dominated by heat capacity changes. Turning now to v, the velocity is proportional to $\sqrt{E/\rho}$, and a decrease in density would imply an increase in ν and thus an increase in κ_p from the Kinetic Theory expression. However, we note that for the thick film HECs, E is decreasing as methane flow rate is increased, and an increase in methane flow rate corresponds to a decrease in ρ in the thin film HECs. We refrain from quantitively comparing the values for E measured in the thick films to ρ measured in the thin films since these properties were measured on separate samples due to experimental limitations of nano-indentation and XRR, respectively, however, we qualitatively expect the general trends to be the same, in that a decreasing E would correspond to the decreasing ρ in the thin film series, and vice versa for the thick film series. Given this, we do not expect the changes in the HEC films in the covalently-bonded regime to be strongly influenced by $v \propto \sqrt{E/\rho}$. Thus, taken together, our results suggest that the changes in thermal conductivity are not primarily driven by changes in phononic properties of the HEC lattice, and changes in C or V in the HECs do not strongly contribute to the observed changes in K as a function of density and methane flow rate.

From this discussion that correlates the atomic, microstructural and mechanical properties of the HEC films to their thermal conductivities, we hypothesize that the changing microstructure, point defect composition (or potential scattering with secondary phases that are precipitating from the excess carbon, described below), and local bonding environment are all contributing to the changes in thermal conductivity of the HECs due to changes in the carrier scattering rates (i.e., changes in the mean free paths, λ), and not as strongly due to changes in C or v. Thus, the observed changes in E and ρ more strongly influence the mean free path as opposed to changes in C or v and resulting phonon energies and velocities. While we have previously discussed the role of crystal quality and grain size on the reduction in thermal conductivity, we turn our attention now to the various defect scattering mechanisms that could drive down the thermal conductivity of the HECs as the methane content in the deposition plasma is

This increase in methane content in the deposition plasma and corresponding net increase in carbon content within the film would generally imply a systematic decrease in carbon vacancies. As carbon vacancies and additional secondary covalently bonded carbonaceous phases will both change and scatter the phonon and electron populations, it should follow suit that lowering the concentration of carbon vacancies would result in an increase of the total thermal conductivity. In the HEC carbon series, however, the total thermal conductivity decreases with increased carbon content even in the single phase carbide regime between $\approx 12 - 16\%$ methane. The total thermal conductivity drops by \approx 17% across a carbon stoichiometry increase of 8%. Thus, we posit that a decrease in phonon-vacancy scattering rates with increased methane content during deposition is not impacting the thermal conductivity of the HEC films as strongly as the increase in phonon scattering rates (and subsequent decrease in thermal conductivity) due to the changing microstructure, point defect composition (or potential

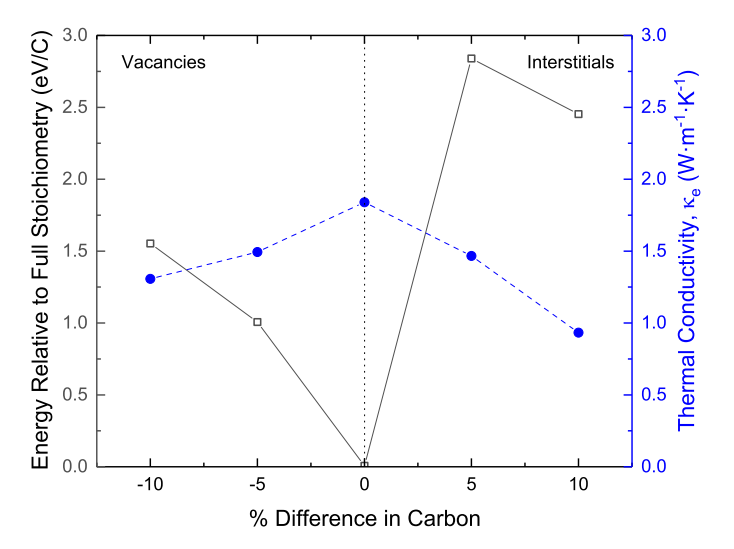


Fig. 6. Defect energies relative to carbon in graphite (solid line, left vertical axis) and the electrical contribution to thermal conductivity (dashed line, right vertical axis) as a function of defect concentration for carbon vacancies and interstitials calculated from DFT and Boltzmann transport theory.

scattering with secondary phases that are precipitating from the excess carbon, described below), and local bonding environment.

The combined analysis of XPS and SEM suggest that while there may be some vacancy filling as carbon content is increased, the non-metal bonded carbon concentrations increase more rapidly with film evolution, up to and exceeding the point of secondary phase formation. Computational analysis suggests that additional carbon content in the carbide lattice is not energetically favorable on the whole. While both vacancy and interstitial concentrations will change, it is not unprecedented to precipitate a secondary graphitic phase before reaching a stoichiometric composition [46,47]. To better understand the defect structure and its influence on the electrical contributions to the thermal conductivity, Density Functional Theory (DFT) calculations together with semi-classical Boltzmann transport theory were used to calculate the energy and electrical conductivity of the fully stoichiometric system, as well as systems containing carbon vacancies and interstitials. Details of the calculations are given in Supplemental Material [25]; results are plotted in Fig. 6. Calculated electrical resistivity has been converted to a thermal conductivity assuming Wiedemann-Franz behavior (assuming $L = L_0$). On the x-axis, -10% and -5% correspond to 4 and 2 missing carbon atoms from a 40 carbon atom supercell, respectively, while 5% and 10% corresponds to 2 and 4 extra interstitial carbon atoms, respectively, in the same system. The energies are calculated from the difference between the fully stoichiometric and defected systems, relative to the chemical potential of carbon μ_c as

$$F^{D} = \frac{[E^{d} - E^{s} - (N^{d} - N^{s})\mu_{c}]}{[N^{d} - N^{s}]}$$
(3)

where E^d and E^s are the DFT energies for the defected and fully stoichiometric systems, respectively, and N^d and N^s are the number of carbon atoms in the defected and fully stoichiometric systems, respectively. The cohesive energy of graphite calculated from DFT as described in Supplemental Material (7.96 eV/atom) is used μ_c [25]. Both the vacancy and interstitial formation energies (solid line, left vertical axis) are positive, suggesting that the fully stoichiometric system has the lowest enthalpy relative to the defected structures. However, the energy for creating interstitial carbon is considerably larger than that for creating a vacancy such that the formation of a second graphitic carbon phase is highly favorable when excess carbon is introduced into the system. These results

are consistent with the experimental results, where carbon indicative of a second phase is measured for high methane flow rates.

For comparison to experimental results, the calculated electrical contribution to the thermal conductivities are plotted in Fig. 6 (dashed line, right vertical axis). The values show relatively little dependence on stoichiometry, with the electrical contribution to thermal conductivity being slightly higher for the ideal system compared to the defected structures. This supports the conclusion based on the experimental data that the large κ_e measured at low flow rates is due to the metallic bonding and high concentration of free electrons. This result also implies that the relative independence of the electronic contribution to thermal conductivity on stoichiometry once the carbide is formed cannot be taken as a measure of defect concentration, but rather other means are needed to quantify carbon defects. This is again consistent with the interpretation of the experimental data.

The trends observed in the electronic contribution to the thermal conductivity and, subsequently, in the phonon contribution can be summarized independently. At the lowest carbon concentrations, electrons are the primary energy carriers, as metallic bonding is predominant. As more carbon is introduced, the phase transforms into a carbide, lowering the free electron concentration to that of metallic covalent crystal. At this point phonons are the dominant energy carriers, and κ_p is increased with increasing carbon content as vacancy concentrations decrease. The effect is weak in general due to simultaneous production of interstitial and graphitic carbon, dampening the effect of vacancy elimination. The onset of secondary phase precipitation introduces more scattering, driving κ_p lower with increasing carbon while κ_e remains constant after the change from primarily metallic bonding to more covalent bonding. A possible cause for this independence is due to the electronic nature of the graphite precipitate. The electronic conductivity of graphite across the basal plane is on the same order [48] to that of the main carbide phase. Thus, while the addition of a secondary phase will affect phonon scattering, it may not affect electron contributions.

An interesting aspect of the observed trend in total thermal conductivity of the HEC materials versus that of their binary counterparts is that the thermal conductivity of HECs decrease with increased carbon content. Previously reported values of carbon stoichiometry effects on the thermal conductivity of binary carbides show that thermal conductivity increases as the relative carbon content increases towards the 1:1 carbon:metal ratio [22–24]. This suggests that the decrease observed in the HEC system could be an intrinsic property of the HECs, related to the bonding environment changes as the system transitions from a primarily metallic bonded to a primarily covalently bonded crystal.

4. Conclusions

In summary, we have investigated the effect of carbon stoichiometry on thermal conductivity of high entropy carbide thin film systems $HfZrTaMoWC_{1-x}$ and $HfZrTaTiNbC_{1-x}$. Structural and compositional characterization of the HfZrTaMoWC_{1-x} show systematic changes in film stoichiometry, phase, modulus and microstructure, all of which impact the thermal conductivity. Low carbon content films are metallic in nature, and electrons are significant thermal carriers. As carbon content increases, the change from a metal to metal carbide lowers κ_e , and the phonon contribution plays a greater role in the thermal conductivity of both HEC systems. While κ_e is minimized, a combination of changes in microstructure, defect concentration and secondary phase formation, and stiffness influence the phononic contribution to thermal conductivity. Our results demonstrate the ability to tune the thermal functionality of high entropy materials through stoichiometries that dictate the type of bonding environment.

Declaration of Competing Interest

The authors declare that they have no known competing financial interests or personal relationships that could have appeared to influence the work reported in this paper.

Acknowledgments

We acknowledge support from Office of Naval Research MURI Program (Grant No. N00014-15-1-2863) and National Science Foundation DMREF Program (Grant No. 1921973). Both nanoindentation and XPS capabilities were provided through the Materials Characterization Laboratory at The Pennsylvania State University Materials Research Institute, State College, PA.

Supplementary material

Supplementary material associated with this article can be found, in the online version, at 10.1016/j.actamat.2020.06.005

References

- [1] E.P. George, D. Raabe, R.O. Ritchie, High-entropy alloys, Nat. Rev. Mater. 4 (8) (2019) 515–534, doi:10.1038/s41578-019-0121-4.
- [2] H.S. Oh, S.J. Kim, K. Odbadrakh, W.H. Ryu, K.N. Yoon, S. Mu, F. Körmann, Y. Ikeda, C.C. Tasan, D. Raabe, T. Egami, E.S. Park, Engineering atomic-level complexity in high-entropy and complex concentrated alloys, Nat. Commun. 10 (1) (2019) 2090, doi:10.1038/s41467-019-10012-7.
- [3] J. Gild, Y. Zhang, T. Harrington, S. Jiang, T. Hu, M.C. Quinn, W.M. Mellor, N. Zhou, K. Vecchio, J. Luo, et al., High-Entropy metal diborides: a New class of high-Entropy materials and a new type of ultrahigh temperature ceramics, Sci. Rep. 6 (October) (2016) 37946, doi:10.1038/srep37946. http://www.nature. com/articles/srep37946
- [4] T.J. Harrington, J. Gild, P. Sarker, C. Toher, C.M. Rost, O.F. Dippo, C. McElfresh, K. Kaufmann, E. Marin, L. Borowski, P.E. Hopkins, J. Luo, S. Curtarolo, D.W. Brenner, K.S. Vecchio, et al., Phase stability and mechanical properties of novel high entropy transition metal carbides, Acta Mater. 166 (2019) 271–280. S135964541831005X
- [5] D.B. Miracle, O.N. Senkov, A critical review of high entropy alloys and related concepts, Acta Mater. 122 (2017) 448–511, doi:10.1016/j.actamat.2016.08.081.
- [6] M.H. Tsai, J.W. Yeh, High-entropy alloys: a critical review, Mater. Res. Lett. 2 (3) (2014) 107–123, doi:10.1080/21663831.2014.912690.
- [7] J.L. Braun, C.M. Rost, M. Lim, A. Giri, D.H. Olson, G. Kotsonis, G. Stan, D.W. Brenner, J.-P. Maria, P.E. Hopkins, G. Katsonis, G. Stan, D.W. Brenner, J.-P. Maria, P.E. Hopkins, Amorphous-like thermal conductivity in single-crystal entropy stabilized oxides via charge induced atomic-scale disorder, Adv. Mater. 30 (2018) 180-5004
- [8] C.M. Rost, E. Sachet, T. Borman, A. Moballegh, E.C. Dickey, D. Hou, J.L. Jones, S. Curtarolo, J.-P. Maria, et al., Entropy-stabilized oxides, Nat. Commun. 6 (2015) 1–18, doi:10.1038/ncomms9485.
- [9] C.M. Rost, Entropy-stabilized oxides: explorations of a novel class of multicomponent materials, North Carolina State University, 2016 Ph.D. thesis. https://repository.lib.ncsu.edu/handle/1840.16/11411?show=full
- [10] X. Yan, L. Constantin, Y. Lu, J. Silvain, M. Nastasi, B. Cui, et al., Hf_{0.2}zr_{0.2}ta_{0.2}nb_{0.2}ti_{0.2}c highentropy ceramics with low thermal conductivity, J. Am. Ceram. Soc. 101 (10) (2018) 4486–4491, doi:10.1111/jace.15779.
- [11] D. Demirskyi, H. Borodianska, T.S. Suzuki, Y. Sakka, K. Yoshimi, O. Vasylkiv, et al., High-temperature flexural strength performance of ternary high-entropy carbide consolidated via spark plasma sintering of TaC, ZrC and NbC, Scr. Mater. 164 (2019) 12–16, doi:10.1016/j.scriptamat.2019.01.024. https://www.sciencedirect.com/science/article/pii/S1359646219300417
- [12] P. Sarker, T. Harrington, C. Toher, C. Oses, M. Samiee, J.-P. Maria, D.W. Brenner, K.S. Vecchio, S. Curtarolo, et al., Novel high-entropy high-hardness metal carbides discovered by entropy descriptors, Nat. Commun. 9 (1) (2018) 4980, doi:10.1038/s41467-018-07160-7.
- [13] L. Feng, W.G. Fahrenholtz, G.E. Hilmas, Y. Zhou, et al., Synthesis of single-phase high-entropy carbide powders, Scr. Mater. 162 (2019) 90–93, doi:10.1016/j.scriptamat.2018.10.049.
- [14] J. Zhou, J. Zhang, F. Zhang, B. Niu, L. Lei, W. Wang, et al., High-entropy carbide: a novel class of multicomponent ceramics, Ceram. Int. 44 (17) (2018) 22014–22018, doi:10.1016/j.ceramint.2018.08.100. https://www.sciencedirect.com/science/article/pii/S0272884218321576
- [15] E. Castle, T. Csanádi, S. Grasso, J. Dusza, M. Reece, et al., Processing and properties of high-Entropy ultra-High temperature carbides, Sci. Rep. 8 (1) (2018) 8609, doi:10.1038/s41598-018-26827-1.
- [16] B. Ye, Y. Chu, K. Huang, D. Liu, et al., J. Am. Ceram. Soc. 102 (3) (2018) 919–923, doi:10.1111/jace.16141.
- [17] R. Cheaito, J.C. Duda, T.E. Beechem, K. Hattar, J.F. Ihlefeld, D.L. Medlin, M.A. Ro-driguez, M.J. Campion, E.S. Piekos, P.E. Hopkins, Experimental investigation of size effects on the thermal conductivity of silicon-germanium alloy thin films, Phys. Rev. Lett. 109 (2012) 195901, doi:10.1103/PhysRevLett.109.195901.

- [18] B. Abeles, Lattice thermal conductivity of disordered semiconductor alloys at high temperatures, Phys. Rev. 131 (1963) 1906–1911.
- [19] F. Körmann, Y. Ikeda, B. Grabowski, M.H.F. Sluiter, et al., Phonon broadening in high entropy alloys, Comput. Mater. 3 (36) (2017) 1–9, doi:10.1038/s41524-017-0037-8.
- [20] A. Giri, J.L. Braun, C.M. Rost, P.E. Hopkins, On the minimum limit to thermal conductivity of multi-atom component crystalline solid solutions based on impurity mass scattering, Scr. Mater. 138 (2017) 134–138, doi:10.1016/j.scriptamat.2017.05.045.
- [21] A. Giri, J.L. Braun, P.E. Hopkins, Reduced dependence of thermal conductivity on temperature and pressure of multi-atom component crystalline solid solutions, J. Appl. Phys. 123 (2018) 015106, doi:10.1063/1.5010337.
- [22] G.V. Samsonov, I.M. Vinickij, Handbook of refractory compounds, 1980. https://www.springer.com/us/book/9781468461015
- [23] H.O. Pierson, Handbook of Refractory Carbides and Nitrides: Properties, Characteristics, Processing, and Applications, Noyes Publications, 1996. https://www.sciencedirect.com/book/9780815513926/handbook-of-refractory-carbides-and-nitrides
- [24] L.G. Radosevich, W.S. Williams, Thermal conductivity of transition metal carbides, J. Am. Ceram. Soc. 53 (1) (1970) 30–33, doi:10.1111/j.1151-2916.1970. tb11994.x.
- [25] See Supplemental Material at xxxx for fabrication and characterization methods and details (including sputtering, XRD, SEM, XPS, nanoindentation, electrical conductivity, and thermal conductivity using TDTR), tabulated property data for the Hf_{0.2}Zr_{0.2}Ta_{0.2}Mo_{0.2}W_{0.2}C_{1-x} and Hf_{0.2}Zr_{0.2}Ta_{0.2}Ti_{0.2}Nb_{0.2}C_{1-x}, thin film heat capacity measurements, thermal conductivity data on a series of control TaC_{1-x} films, and further information of our density functional theory simulations
- [26] D.G. Cahill, Analysis of heat flow in layered structures for time-domain thermoreflectance, Rev. Sci. Instrum. 75 (12) (2004) 5119–5122.
- [27] A.J. Schmidt, Pump-probe thermoreflectance, Ann. Rev. Heat Transf. 16 (2013) 159–181.
- [28] G. Wiedemann, R. Franz, Ueber die warme-leitungsfahigkeit der matalle, Ann. Phys. 165 (1853) 497–531.
- [29] R.E.B. Makinson, The thermal conductivity of metals, Math. Proc. Cambridge Philos. Soc. 34 (3) (1938) 474–497, doi:10.1017/S0305004100020442. https://www.cambridge.org/core/article/thermal-conductivity-of-metals/9815CCE36F6926B189F90503C5B0AADE
- [30] W.S. Williams, High-temperature thermal conductivity of transition metal carbides and nitrides, J. Am. Ceram. Soc. 49 (1966) 156–159.
- [31] W.S. Williams, The thermal conductivity of metallic ceramics, JOM J. Miner. Metals Mater. Soc. 50 (1998) 62–66.
- [32] Q. Zheng, A.B. Mei, M. Tuteja, D.G. Sangiovanni, L. Hultman, I. Petrov, J.E. Greene, D.G. Cahill, Phonon and electron contributions to the thermal conductivity of vn_x epitaxial layers, Phys. Rev. Mater. 1 (2017) 065002, doi:10. 1103/PhysRevMaterials.1.065002.
- [33] X. Zheng, D.G. Cahill, R. Krasnochtchekov, R.S. Averback, J.C. Zhao, High-throughput thermal conductivity measurements of nickel solid solutions and the applicability of the Wiedemann-Franz law, Acta Mater. 55 (2007) 5177–5185.
- [34] A.D. Avery, S.J. Mason, D. Bassett, D. Wesenberg, B.L. Zink, Thermal and electrical conductivity of approximately 100-nm permalloy, ni, co, al, and cu films and examination of the wiedemann-franz law, Phys. Rev. B 92 (2015) 214410, doi:10.1103/PhysRevB.92.214410.
- [35] N.W. Ashcroft, N.D. Mermin, Solid State Physics, Saunders College, Fort Worth, 1976.
- [36] A. Srivastava, B.D. Diwan, Elastic and thermodynamic properties of divalent transition metal carbides MC (M = Ti, Zr, Hf, V, Nb, Ta), Can. J. Phys. 90 (4) (2012) 331–338, doi:10.1139/p2012-021.
- [37] D. Connétable, First-principles study of transition metal carbides, Mater. Res. Express 3 (12) (2016) 126502, doi:10.1088/2053-1591/3/12/126502.
- [38] W.S. Williams, Electrical properties of hard materials, Int. J. Refract. Met. Hard Mater. 17 (1) (1999) 21–26, doi:10.1016/S0263-4368(99)00005-0. http://www.sciencedirect.com/science/article/pii/S0263436899000050
- [39] J. Ravichandran, W. Siemons, D.W. Oh, J.T. Kardel, A. Chari, H. Heijmerikx, M.L. Scullin, A. Majumdar, R. Ramesh, D.G. Cahill, et al., High-temperature thermoelectric response of double-doped SrTiO₃ epitaxial films, Phys. Rev. B 82 (2010) 165126, doi:10.1103/PhysRevB.82.165126.
- [40] Y.-F. Kao, S.-K. Chen, T.-J. Chen, P.-C. Chu, J.-W. Yeh, S.-J. Lin, Electrical, magnetic, and hall properties of Al_xcocrfeni high-entropy alloys, J. Alloys Compd. 509 (5) (2011) 1607–1614, doi:10.1016/j.jallcom.2010.10.210.
- [41] P.G. Klemens, R.K. Williams, Thermal conductivity of metals and alloys, Int. Metals Rev. 31 (1986) 197–215.
- [42] K.E. Meyer, R. Cheaito, E. Paisley, C.T. Shelton, J.L. Braun, J.-P. Maria, J.F. Ihle-feld, P.E. Hopkins, Crystalline coherence length effects on the thermal conductivity of MgO thin films, J. Mater. Sci. 51 (23) (2016) 10408–10417, doi:10.1007/s10853-016-0261-5.
- [43] D.-W. Oh, J. Ravichandran, C.-W. Liang, W. Siemons, B. Jalan, C.M. Brooks, M. Huijben, D.G. Schlom, S. Stemmer, L.W. Martin, A. Majumdar, R. Ramesh, D.G. Cahill, Thermal conductivity as a metric for the crystalline quality of SrTiO₃ epitaxial layers, Appl. Phys. Lett. 98 (2011) 221904.
- [44] G.A. Slack, Nonmetallic crystals with high thermal conductivity, J. Phys. Chem. Solids 34 (1973) 321–335.
- [45] W.G. Vincenti, C.H. Kruger, Introduction to Physical Gas Dynamics, Krieger Publishing Company, Malabar, FL. 2002.

- [46] U. Jansson, E. Lewin, Sputter deposition of transition-metal carbide films -a critical review from a chemical perspective, Thin. Solid Films 536 (2013) 1–24, doi:10.1016/j.tsf.2013.02.019. http://www.sciencedirect.com/science/article/ pii/S004060901300268X
- [47] P. Malinovskis, S. Fritze, L. Riekehr, L. von Fieandt, J. Cedervall, D. Rehnlund, L. Nyholm, E. Lewin, U. Jansson, Synthesis and characterization of multicomponent (crnbtatiw)c films for increased hardness and corrosion resis-
- tance, Mater. Des. 149 (2018) 51-62, doi:10.1016/j.matdes.2018.03.068. http:
- //www.sciencedirect.com/science/article/pii/S0264127518302594

 [48] D.R. Lide, CRC Handbook for Chemistry and Physics. Internet Version, 89, CRC Press/Taylor and Francis, Boca Raton, 2008.